Homeostatic scaling is driven by a translation-dependent degradation axis that recruits miRISC remodelling

Balakumar Srinivasan[1#], Sarbani Samaddar[1#], Sivaram V.S. Mylavarapu[2], James P. Clement[3] and Sourav Banerjee[1§]

1. National Brain Research Centre, NH-8. Nainwal Mode, Manesar-122052, Haryana, India

2. Regional Centre for Biotechnology, NCR-Biotech Science Cluster, Faridabad-Gurgaon Expressway, Faridabad-121001, Haryana, India

3. Neuroscience Unit, Jawaharlal Nehru Centre for Avanced Scientific Research, Jakkur, Bengaluru-560064, Karnataka, India.

# These authors contributed equally to this work

§ Correspondence

souravnbrc@gmail.com OR sourav@nbrc.ac.in (S.B)

Abstract

Homeostatic scaling in neurons involve substantial proteome remodelling. Although dynamic changes to the proteome have been attributed to either translational or degradative control individually, there remains a lack of insight towards understanding how the interplay between translation and degradation modules effectuate cellular proteostasis during scaling. Here, we report that a mutual co-dependence of the two apparatus drive synaptic homeostasis in an RNA-dependent manner. We observed that abrogation of either translation or proteasomal activity prevents homeostasis and delineated the spatial features of their association. Members of the translation apparatus such as eIF4E, active forms of p70S6 kinase and miRISC-associated MOV10 were found to remain spatially linked with subunits of the catalytically active 26S proteasome subunits such as Rpt1, Rpt3, Rpt6, α7 and E3 ligase Trim32 on polysomes. We identified that paradigms of chronic downscaling involve miRISC remodelling and entails the degradation of MOV10 *via* the mTOR-dependent translation of Trim32. miRISC remodelling alone is sufficient to invoke downscaling through the removal of post-synaptic AMPA receptors. Our finding proposes a multifaceted model, where synaptic scaling is regulated by compositional changes in the miRISC *via* protein-synthesis-driven protein degradation.

Introduction:

Neurons employ a unique stratagem, known as synaptic scaling, to counter the run-away excitation and subsequent loss of input specificity that arise due to Hebbian changes; they rely on a compensatory remodelling of synapses throughout the network while maintaining differences in their synaptic weightage (1–8). A complex interplay of sensors and effectors within neurons serve to oppose global fluctuations in a network by modifying post-synaptic glutamatergic currents in a cell-autonomous manner (9–12). In this context, ‘sensors’ are classified as molecules that sense deviations in the overall network activity, and ‘effectors’ scale the neuronal output commensurately.

Few molecular sensors of scaling have been identified to date; the eukaryotic elongation factor eEF2 and its dedicated kinase, eEF2 kinase or CamKIII are the two reported thus far (13). However, there remains a huge chasm in identifying the repertoire of molecular cascades that serve to link events where neurons sense deviations in the network firing rate and subsequently initiate the scaling process. One such cascade is the mTORC1 (mammalian Target Of Rapamycin Complex-1) signalling pathway that regulates

presynaptic compensation by promoting BDNF synthesis in the post-synaptic compartment (14, 15). In contrast, AMPA-receptors (AMPARs) have been identified, by overwhelming consensus, to be the predominant “end-point-effectors” in all paradigms of synaptic scaling (16–19). Unlike NMDARs, AMPARs undergo *de novo* translation during network destabilizations (20) and chronic changes in the post-synaptic response during scaling has been attributed to the re-distribution of surface AMPARs (GluA1 and GluA2 subunits) (21). Among the key modifiers of AMPAR expression, miRNAs are known to play pivotal roles in synaptic scaling (22–25) . Relief from translational repression by miRNAs necessitates that mRNAs exit the functional miRISC, which entails that the latter undergo dynamic changes in its composition (26, 27).

The requirement for discrete sets of sensors and effectors is fulfilled within neurons through varied mechanisms including transcription, translation and ubiquitin-mediated proteasomal (UPS) degradation (10, 13, 28–31). An enhanced degradation of post-synaptic-density (PSD) proteins including GluA1 and GluA2 has been observed in contexts of altered network excitability (28) whereas complete inhibition of UPS activity was shown to occlude synaptic compensation (29). The integral role of *de novo* translation in sculpting the neuronal proteome was recently highlighted when proteomic analysis of neurons undergoing upscaling and downscaling revealed a remarkable diversity of newly synthesized proteins. Of particular interest was the significant enrichment in the expression of the proteasome core complex during the downscaling of synaptic activity (30, 31). The demand for the translation of proteasome complexes imply that proteasomes work alongside translation mechanisms during downscaling to drive the downregulation of surface AMPARs (sAMPARs). Reports documenting the co-localization of ribosomes and the proteasome in neuronal dendrites (32, 33) further emphasize the possibility that these two opposing machineries physically interact within the post-synaptic microcosm. However, several questions remain unexplored in this context, such as a) What are the spatial attributes of the translation and degradation events that shape the proteome during scaling? b) which process among translation and degradation takes precedence ? c) what are the signalling mechanisms that connect events of ‘sensing’ the bicuculline mediated hyperactivity and the final downregulation of AMPARs?

Here, we demonstrate a defined mechanism of synaptic scaling accomplished through the remodelling of miRISC *via* the synchronous effects of translation and proteasome-mediated degradation. We observe that isolated inhibition of either translation or proteasomal activity offsets synaptic homeostasis and restoration of homeostasis

necessitates the coordination of both processes. We provide unprecedented empirical evidence that the translation and degradation apparatus remain associated with each other and identify this association to be RNA-dependent and facilitated by a proteasome-associated chaperone protein HspA2. We propose that in contexts of chronic hyperactivity, it is translation that drives proteasomal degradation; hyperactivity induced translation of the E3 ligase Trim32 promotes the degradation of MOV10, both members of the miRISC. We find that the miRISC is a key node in the translation-degradation axis, with mTORC1 being the upstream molecular component, and the re-distribution of AMPARs being the final effectors of downscaling.

Results

Synaptic homeostasis requires both protein synthesis and degradation

To test the synergistic effect of translation and degradation in synaptic homeostasis, we measured miniature EPSCs (mEPSCs) from cultured hippocampal neurons (DIV 18-24) after pharmacological inhibition of protein synthesis (anisomycin, 40µM) and proteasomal activity (lactacystin, 10µM) for 24 hours. Application of either lactacystin or anisomycin significantly increased (2.99± 1.23 pA, $p<0.02$) and decreased (5.76± 0.5 pA, $p<0.01$) mEPSC amplitudes respectively. Co-application of both restored mEPSC amplitudes as compared to vehicle treated neurons (Figure 1A-B). The frequency of mEPSCs remained unaltered upon inhibition of translation and proteasome blockade either alone or in combination (Figure 1C), suggesting that this could be a post-synaptic phenomenon. We stimulated synaptic downscaling using bicuculline (10µM, 24 hr) and observed that like previous reports (30), here too, chronic application of bicuculline lead to a significant decrease in mEPSC amplitudes (5.56 ± 0.31 pA, $p<0.01$) without any detectable change in frequencies (Figure 1D-F). Remarkably, the extent of decrease in mEPSC amplitudes within bicuculline-treated neurons recapitulated the decrease observed in neurons where translation was blocked (bicuculline treated neuron 5.56 ± 0.31 pA decrease *vs.* anisomycin treated neuron 5.76 ± 0.5 pA decrease) (Figure 1B and 1E). The dual application of bicuculline and anisomycin did not result in any significant change in mEPSC amplitudes when compared to neurons treated with bicuculline alone (Figure 1D-E). This confirms that, rather than inducing a synergistic effect, chronic inhibition of protein synthesis in itself is sufficient to induce downscaling and could potentially override the effect observed due to bicuculline.

Disruption of proteasome function by lactacystin during bicuculline-treatment led to a significant increase in mEPSC amplitudes (9.45 ± 0.25 pA increase as compared to bicuculline treated neurons, $p<0.01$) without altering frequencies (Figure 1E-F). The increase was effectively more than basal activity of vehicle-treated neurons (3.88 ± 0.28 pA, $p<0.01$) and mimicked the increase in mEPSC amplitudes brought by lactacystin alone (Fig 1B and 1E). Although the influence of lactacystin on mEPSC amplitudes is opposite to that of anisomycin, their individual effects override that of bicuculline in each case. However, co-application of both during bicuculline-induced hyperactivation produced mEPSC amplitudes comparable to vehicle treated neurons (Figure 1E).

Synchronized translation and degradation regulates AMPAR distribution during scaling

We measured the surface expression of GluA1 and GluA2 (sGluA1/A2) to identify how concerted mechanisms of synthesis and degradation influence the distribution of surface AMPARs (sAMPARs) during scaling. Neurons (DIV 21-24) were live-labelled using N-terminus specific antibodies against GluA1 and GluA2 following bicuculline treatment, either alone or in presence of both anisomycin and lactacystin for 24 hours and synapses marked by PSD95. The surface expression of sGluA1/A2 in excitatory neurons was significantly decreased following network hyperactivity (50.6 ± 6.68%, $p<0.01$ for sGluA1 and 26.1 ± 6.62%, $p<0.01$ for sGluA2) (Figure 2A-D, S1 A-B). Consistent with our electrophysiological data, inhibition of both the translation apparatus and the proteasome in bicuculline-treated neurons significantly increased sGluA1/A2 levels (133.95 ± 8.77 % , $p<0.01$ for sGluA1, 53.17 ± 6.44%, $p<0.0001$ for sGluA2) when compared to neurons treated with bicuculline alone (Figure 2C-D). To reaffirm whether they are indeed the end-point effectors of synaptic downscaling, we used $GluA2_{3Y}$, a synthetic peptide derived from the GluA2 carboxy tail of AMPA receptors to block the endocytosis of the AMPARs (16), effectively ensuring the number of AMPARs to remain unchanged throughout 24 hours. Consistent with previous studies, no significant changes in mEPSC amplitudes were detected upon inhibition of GluA2 endocytosis during chronic application of bicuculline ($GluA2_{3Y}$ treated neuron 11.18 ± 1.06 pA *vs.* $GluA2_{3Y}$ + bicuculline treated neuron 12.25 ± 1.15 pA, $p<0.49$) (Figure 2E-F). Application of $GluA2_{3Y}$ did not alter mEPSC amplitudes as compared to vehicle treated neurons ($GluA2_{3Y}$ treated neuron 11.18 ± 1.06 *vs.* vehicle treated neurons 11.82 ± 0.24 pA) (Figure S1C-D), nor any change observed between neurons treated with $GluA2_{3Y}$ and those treated with both lactacystin

and anisomycin in presence or absence of bicuculline (Figure 2F-G). mEPSC frequencies remained unaltered throughout while mEPSC amplitudes in each condition was similar to that of control neurons (Figure 2G, S1E).

RNA-dependent tethering of the proteasome and translation regulators

To evaluate the interaction between the translation machinery and the 26S proteasome, we analyzed polysomes from the hippocampus (8-10 week old rat) and assessed whether the sedimentation pattern of the proteasomes match with those of actively translating, polyribosome-associated mRNA fractions. We observed that several components of the proteasomal machinery such as α7 subunit of 20S; Rpt1, Rpt3 and Rpt6 subunits of the 19S proteasome co-sedimented with translation initiation factors such as eIF4E and p70S6 kinase, the regulatory kinase of mTORC1-mediated protein synthesis within actively translating polysomes (Figure 3A-B, S2A). We also detected the polysomal distribution of MOV10, an RNA binding protein known to be poly-ubiquitinated upon synaptic activation (26), and Trim32, an E3 ligase, both components of the miRISC (34, 35) (Figure 3A-B). RNAse or EDTA treatment of cytoplasmic lysates prior to density gradient fractionation led to a complete collapse of the polysome profile, parallelly shifting the sedimentation of the proteasome subunits, E3 ligase, translation regulators and RNA binding proteins to the lighter fractions (Figure 3C-F, S2B-C). The disruption of association between the translational and proteasomal modules on RNAse and EDTA treatment suggests that RNAs act as scaffolds for their interaction. These observations ruled out a possible causality for the observed co-sedimentation due to similar densities of protein complexes associated with translation and proteasome machineries. Furthermore, we observed that the polysome-associated 26S proteasome is catalytically active as detected by its ability to cleave a fluorogenic proteasome substrate that is blocked by proteasome inhibitor epoxymycin (Figure 3G-H, S2D).

Proteasome and the regulators of translation directly interact with each other within excitatory neurons.

Co-sedimentation of proteasome subunits and protein-synthesis regulators in polysome fractions lead us to enquire whether the two apparatus directly interact with each other. To evaluate this, we immunoprecipitated the 19S proteasomal complex using Rpt6 antibody from hippocampal neurons. We observed the co-precipitation of eEF2, a translation

elongation factor that functions as a “sensor” of change in network activity (Figure 4A). Interestingly, we also found that p70S kinase as well as its phosphorylated form- a known regulator of the mTORC1-dependent protein synthesis (36) co-precipitated with the 19S proteasome (Figure 4A). We further analyzed the proteins interacting with polysomes within excitatory neurons by expressing Hemagglutinin (HA) tagged ribosomal protein Rpl22 (HA-Rpl22) that gets incorporated into polysomes (37, 38) (Figure 4B-D, S2E). Our western blot analysis of HA-Rpl22 affinity-purified protein complex showed that Rpt6 directly interacts with Trim32 and MOV10, (Figure 4E). The interaction of MOV10 with ribosomes is crucial as it gives credence to the association of miRNAs with polysomes, as per previous reports (39). Immunoprecipitation of MOV10 from hippocampal neurons allowed us to detect the co-precipitation of both Argonaute (Ago) and Trim 32, confirming that the latter is an integral component of the Ago-containing miRISC (Figure 4F). We also detected the chaperone protein HspA2 in the HA-affinity purified fraction along with Rpt6 (Figure 4G), suggesting that HspA2 could tether proteasomes to actively translating transcripts.

Protein synthesis drives mTORC1-dependent proteasomal degradation to cause miRISC remodelling during synaptic downscaling

Association between MOV10 and Trim32, all members of the miRISC, and their direct interaction with protein synthesis and degradation machineries led us to analyze whether concerted translation and degradation during bicuculline induced chronic network hyperactivity could influence miRISC remodelling. Bicuculline treatment of hippocampal neurons (DIV 18 - 21) significantly enhanced (101.7 ± 71.61% increase, $p<0.01$) Trim32 with a concomitant decrease (65.94 ± 27.36% decrease, $p<0.02$) in MOV10 (Figure 5A-C). The increase in Trim32 expression post bicuculline treatment was blocked by anisomycin and surprisingly resulted in the inhibition of MOV10 degradation (199.6 ± 122.27% protected MOV10, $p<0.03$) (Figure 5C).Treatment with lactacystin resulted in the expected protection of MOV10 from degradation (151.71 ± 97.7% MOV10 protected, $p<0.01$); whereas there remained no change in the Trim32 expression levels (Figure 5B). Moreover, co-application of lactacystin and anisomycin during bicuculline-induced hyperactivity changed the expression of MOV10 and Trim32 commensurate to basal levels (Figure 5B-C). Furthermore, knockdown of Trim32 (85.5 ± 20.3% knockdown, $p<0.01$) by shRNA-mediated RNAi enhanced the expression of MOV10 (44.7 ± 20.29% increase, $p<0.01$) (Figure 5D-F), suggesting that Trim32 translation drives the proteasome-mediated

degradation of MOV10 and that it maybe sufficient for MOV10 ubiquitination and subsequent degradation.

Bicuculline-treatment of hippocampal neurons in the presence of rapamycin (100nM, 24 hr), a selective inhibitor of mTORC1, completely abolished chronic hyperactivity-driven Trim32 synthesis (16.5 ± 19.6% increase as compared to control, p=0.19) (Figure 5G-I) and consecutive MOV10 degradation (8.2 ± 12.27% decrease as compared to control, p=0.06) (Figure 5G-I). Rapamycin treatment alone did not alter the expression patterns of Trim32 and MOV10 (Fig 5G-I). This lead us to hypothesize that mTORC1 pathway acts upstream of Trim32, serving to regulate it's synthesis in response to bicuculline. Chronic bicuculline treatment lead to a significant enhancement of p70S6 kinase phosphorylation (92.07 ± 47.93 % increase, p<0.001) which was blocked by rapamycin (Figure S2F-G), indicating that the mTORC1 signalling cascade is key in effectuating bicuculline-induced synaptic downscaling.

Consistent with our data, we observed that co-incubation of rapamycin and bicuculline prevented the decrease in mEPSC amplitudes (2.47 ± 0.26pA increase as compared to bicuculline treated neurons, p<0.01) but not frequencies (Figure 5J-L). Just as above, rapamycin treatment alone has no effect, indicating that chronic hyperactivity acts as a triggering point for mTORC1 activation (Figure 5K-L) and this subsequently plays a role in driving TRIM32 translation.

MOV10 degradation is sufficient to invoke downscaling of AMPARs

MOV10 degradation in response to chronic bicuculline treatment, made us question whether it's loss alone was sufficient to cause pervasive changes in the miRISC and bring about synaptic downscaling. We mimicked hyperactivity-driven MOV10 degradation by lentivirus-mediated RNAi of MOV10. Intensity of sGluA1/A2 puncta that co-localized with PSD95 was analyzed following MOV10 knockdown (DIV21-24). We observed that loss of MOV10 significantly reduced the expression of sGluA1 (35.03 ± 9.35 % for shRNA#1, p<0.01 and 58.38 ± 10.27 % for shRNA#2, p<0.01) and sGluA2 (49.4 ± 12.9% for shRNA#1, p<0.01) at the synapses (Figure 6A-D, S3 A–D), that recapitulated the re-distribution of sGluA1/sGluA2 in neurons under chronic bicuculline treatment (Figure 2C-D). The knockdown of MOV10 significantly reduced mEPSC amplitudes (4.05 ± 0.23 pA for shRNA#1 and 3.48 ± 0.24 pA for shRNA#2, p<0.01) but not frequencies (Figure 6E-G), an observation that mirrors synaptic downscaling following bicuculline treatment (Figure 1E). We have used two shRNAs against MOV10 for its effective knockdown (data not

shown) and also a non-targeting shRNA to eliminate the possibility of an off-target effect (control RNAi). Taken together, our data demonstrates that bicuculline-induced downscaling of synaptic strength happens *via* a translation-dependent proteasomal degradation of MOV10 (Figure 7).

Discussion

Several studies have documented the individual role of translation and proteasomal degradation in regulating protein turnover during homeostatic scaling (20, 28, 29), but there remains inconclusive evidence elucidating whether proteomic remodelling recruits the simultaneous participation of both machinaries. The most significant work addressing this possibility was done recently, where proteins of both the translational and the proteasomal apparatus was found to undergo *de novo* synthesis at different time-points during downscaling (31). We used a paradigm of chronic network hyperactivity to invoke downscaling and determined a new RNA-dependent, translation-driven degradation axis that involves the turnover of Trim32 and MOV10, both components of the miRISC. Bicuculline-induced downscaling resulted in the mTORC1-mediated enhancement of Trim32 synthesis which drives the subsequent degradation of MOV10, resulting in the loss of AMPARs from the post-synaptic membrane.

Participation of both protein synthesis and degradation drives AMPAR-mediated synaptic downscaling

Chronic application of bicuculline along with either lactacystin or anisomycin lead to alterations of mEPSC amplitudes that exactly mirrored observations where bicuculline is absent wherease mEPSC frequencies remained unaltered in all conditions (Figure 1). Thus, the effects of bicuculline-induced changes to the existing proteome were overshadowed by those accomplished by the individual action of the proteasome or the translation machinery (Figures 1).The importance of these observations is multi-faceted; it establishes that, a) congruent protein synthesis and degradation pathways regulate synaptic scaling; b) the constancy of the proteomic pool renders the effect of any network destabilizing stimuli to be redundant, and c) long-term changes in the proteome predominantly affects the physiology of the post-synaptic compartment.

Our observations reinforce previous findings in Hebbian plasticity; wherein, protein synthesis during LTP/LTD was required to counter the changes in the proteomic pool triggered by protein degradation. The blockade of L-LTP accomplished by inhibiting protein synthesis was revoked on the simultaneous application of proteasomal blockers and translational inhibitors (40). Abrogation of proteasomal activity allowed mGluR-dependent LTD to proceed even in the absence of protein synthesis (41). The overall maintenance of the proteome through the dynamic remodelling of the translation pool has been termed as cellular 'proteostasis' (42). As LTP and LTD modify the cellular proteome through the simultaneous recruitment of protein synthesis and degradation; it stands to reason that homeostatic scaling mechanisms may also employ a functional synergy of the two to recompense for the changes brought about by unconstrained Hebbian processes.

Our data emphasises the dual requirement of translation and proteasome-dependent degradation in the reduction of the surface abundance of AMPARs and associated AMPAR-currents upon chronic bicuculline treatment (Figure 2). AMPAR-mediated currents decrease more than NMDAR currents during chronic network hyperactivity (17, 21) and unlike NMDARs, the turnover of AMPARs is translation-dependent (43). Similar to the observations in synaptic upscaling (16), the inhibition of GluA2-endocytosis by $GluA2_{3Y}$ peptide also blocked synaptic down scaling (Figure 2); reinforcing that AMPARs indeed remain the end-point effectors despite changes to the proteome. Although we have detected hyperactivity-driven reduction in sGluA1/A2, our data indicates that the contribution of GluA2 containing AMPARs in down scaling is physiologically more pertinent.

RNA-dependent association of the translation and degradation apparatus underlie their functional coherence

Polysome analysis in the presence of RNAse is indicative of an RNA-dependent direct interaction between translation and degradation (Figure 3-4) . Such co-localization of ribosomes and catalytically active proteasomes in neuronal subcompartments suggest that this association is necessary for translation and proteasomal degradation to work in tandem to ensure dynamicity of the proteome during network-driven hyperactivity. How are protein synthesis and degradation machineries tethered to actively translating mRNAs? We have identified that HspA2 (Hsp70 family), a chaperone protein, remains tethered to proteasomes (Figure 4). Hsp70 family of proteins is known to influence both the synthesis

and degradation of proteins by their association with 26S proteasomal subunits (44) and translation initiation factors (45). Therefore, our observation places HspA2 in a pivotal position to control proteome remodelling during synaptic homeostasis.

mTORC1-mediated Trim32 synthesis precedes MOV10 degradation during homeostatic downscaling

The co-incident detection of MOV10 and miRNAs from polysome fractions purified from neurons (27, 39) give credence to the existence of a tripartite (miRISC – proteasome complex – translation apparatus) regulatory axis underlying scaling. Under the chronic influence of bicuculline, synthesis of the E3 ligase Trim32 precedes the degradation of MOV10, the alternative possibility that MOV10 degradation leads to increased *de novo* translation of Trim32, is not supported, since protein synthesis inhibition by anisomycin leads to MOV10 rescue (Figure 5). This instance of translation-driven, proteasome-dependent degradation is distinct from the recently reported mechanism of proteostasis achieved by the activity-dependent co-translational degradation of newly synthesized peptides involving membrane-anchored 20S proteasome (46).

What post-synaptic signalling cascade triggers Trim32 translation? We find that chronic bicuculline induction triggers the mTORC1-dependent synthesis of Trim32, and the concommitant decrease of MOV10 (Figure 5). Inhibition of mTOR signalling blocks bicuculline induced downscaling, suggesting that it requires the post-synaptic cellular machinary to exploit members of the mTOR pathway to achieve homeostasis.

Degradative control of miRISC remodelling underlies homeostatic scaling

Most studies have focused on the influence of single miRNAs in regulating AMPAR distribution during scaling, however, they have been inadequate in providing a holistic view of the miRNA-mediated control of synaptic scaling (22–25). We found that loss of MOV10 function, single-handedly accounted for the loss of sGluA1/A2, accompanied by commensurate decrease in mEPSC amplitudes, thus effectively recapitulating the post-synaptic events during downscaling (Figure 6). How AMPARs are downregulated post chronic bicuculline induction remains an open-ended question; we believe that MOV10-dependent miRISC remodelling may affect multiple cellular processes which regulate the expression, trafficking, post-translational modification and distribution of AMPARs in the

post-synaptic compartment (47, 48). Significantly, homeostatic downscaling is a key attribute observed in excitatory neurons during sleep wherein synapses undergo pervasive remodelling by a protein kinase A dependent dephosphorylation and removal of surface AMPA receptors in order to aid consolidation of contextual memory (49). The kinetics of miRISC-dependent proteome remodelling during sleep and its correlation with synaptic events may be explored further in order to understand the extent to which syncretic translation and degradation processes influence the temporal resolution of scaling during such physiological functions.

Materials and Methods

Primary neuronal culture

Hippocampal neuronal cultures from rat (Sprague-Dawley) were prepared and maintained as described previously (50). Neurons were maintained in Neurobasal medium (Gibco) containing B27 supplements (Gibco) at 5% CO_2 / 37°C up to 25 days prior to commencement of experiments. Animal experiments were performed with the approval of the Institutional Animal Ethics (IAEC) committee of National Brain Research Centre.

Lentivirus production and transduction

Lentivirus preparations and transduction into hippocampal neuronal cultures were performed as described previously (26). Validated shRNA against Trim32 (TATACCTTGCCTGAAGATC) (34) was cloned into MluI and ClaI sites of pLVTHM vector (Addgene) and verified by sequencing. pLVTHM vectors containing MOV10 shRNA cassettes (sh#1:TTATACAAGGAGTTGTAGGTG) or (sh#2: ACTTAGCTCTAGTTCATAACC) (26) and non-targetting control (ATCTCGCTTGGGCGAGAGTAAG) were used for lentivirus preparation.

To perform RNAi, hippocampal neurons at Days *In Vitro* (DIV) 14-15 were infected with lentivirus expressing shRNAs against MOV10, Trim32 and non-targeting control respectively. Neurons were incubated up to DIV25 prior to surface labeling,

electrophysiology and biochemical experiments. Viral infected neurons were tracked by EGFP expression for electrophysiology and imaging experiments.

Surface labeling of GluA1/A2

Surface expression of AMPAR subunits (GluA1 or GluA2) was analyzed by live-labeling of hippocampal neurons (DIV 21 – 24) with primary antibodies against surface epitopes of GluA1 (Millipore) or GluA2 (Millipore) as described previously (51).

Confocal Imaging and Image Analysis

Hippocampal neurons were imaged using a Leica TCS SP8 point scanning confocal microscope with a Leica Plan Apochromat 63X NA = 1.4 oil immersion objective at 1024 × 1024 pixel resolution. High magnification images were captured using 2X optical zoom.

High magnification images, captured from confocal microscopy, were analyzed to observe the intensity of GluA1/A2 expression colocalizing with PSD95 (and GFP for MOV10 RNAi experiments). Images from the different channels were stacked and projected at maximum intensity using ImageJ (NIH). These images were then analyzed using custom written Matlab (Mathworks) programs.

Polysome fractionation and TCA precipitation of polysome fractions:

Polysomes from the hippocampi of 8-10 week old SD rats were analyzed following previous protocol (52). Tri-chloroacetic acid (TCA) was added to polysome fractions at 25% of their volume, incubated on ice for 30 mins post TCA addition and polysome assciated proteins were precipitated by centrifugation at 13,000g for 30 mins at 4^0C. The pellets were washed with ice-cold acetone (Merck), dried and resuspended in Laemmli buffer.

Proteasome activity assay

Proteasome activity present in monosome and polysome fractions were analyzed by 20S Proteasome Assay Kit (Enzo Lifesciences) as per manufacturer's protocol. Briefly, 20S proteasome chymotrypsin-like activity was tested by incubating 80µl of each fraction with Suc-LLVY-AMC fluoregenic peptide substrate with or without epoxymycin (500nM) for 15 minutes at 30ºC. Fluorescence was detected by fluoremeter (Tecan).

Immunoprecipitation from HA-Rpl22 mice:

HA-tagged ribosomes from adult male mice were immunoprecipitated following previous protocol (37) The immunoprecipitated protein complex were resuspended in Laemmli buffer for Western Blot analysis.

Immunoprecipitation of 26S proteosome subunits and MOV10 from rodent hippocampus:

Immunoprecipitation of 26S proteosome and MOV10 containing RISC were performed using rat hippocampus (8-10 week old) from male Sprague Dawley rats. The immunoprecipitated samples were resuspended in Laemmli buffer and for western blot analysis.

Western Blot for immunoprecipitated samples and polysomes:

Immunoprecipitated samples were analyzed as per previous protocols (26) using MOV10 (Bethyl Lab), Trim 32 (Abcam), Ago (Millipore); eEF2, eIF4E, p70S6 kinase, phospho-p70S6 kinase (Cell Signalling Technologies); 19s subunits Rpt1, Rpt3 Rpt6, α7 subunit of 20S core (Enzo Lifesciences); Tuj1 (Sigma) and GAPDH (Sigma).

Blots were detected using standard chemiluminescence (Millipore) detection.

Whole-Cell Voltage Clamp Recordings:

Primary hippocampal neurons (DIV18-25) were used for patch clamp recordings. Glass pipettes (~3-8MΩ) were used in the recordings to patch the neurons and were clamped at -70mV. Pipettes were back-filled with internal solution (100mM Cesium gluconate, 0.2mM EGTA, 5mM MgCl2, 2mM ATP, 0.3mM GTP, 40mM HEPES, pH 7.2) and neurons were recorded in the bath solution (119mM NaCl, 5mM Kcl, 2mM CaCl2, 2mM MgCl2, 30mM glucose, 10mM HEPES, pH7.4 with 1μM tetrodotoxin and 10μM Bicuculline). mEPSC events were analyzed from 300s of recording from each neuron and were filtered and analyzed offline using pClamp10.5 software and MATLAB.

Statistical Analysis:

Statistical Analyses were performed for all experiments. Whole cell patch clamp amplitudes and frequencies were analyzed using one-way ANOVA with post-hoc Fisher's LSD test to test pairwise differences across the groups. Imaging and western blot data were analyzed for statistical significance using one-way ANOVA with post-hoc Fisher's LSD test. Western blot data related to RNAi experiment was analyzed using unpaired t-test with Welch's correction. Data is reported as absolute differences in mean ± SEM for electrophysiology data or percent differences in mean ± SEM for imaging and western blot data between groups.

The detailed methodology for all precudures are described in Supporting Information.

Author Contributions

S.B and S.S designed the study. S.S., and B.S. performed all experiments. S.S., B.S., and S.B. analyzed the data. J.P.C. provided critical comments on electrophysiology experiments and manuscript. S.V.S.M gave comments on manuscript. S.S. and S.B wrote the manuscript.

Acknowledgement:

We thank Addgene for lentiviral vectors, Ken Kosik for MOV10 shRNA constructs, microscope facility of Regional Centre for Biotechnology, India, Utsav Mukherjee for confocal imaging, Rohini Roy for analyzing efficacy of RNAi and Premkumar Palanisamy for maintenance of transgenic animals. This work is supported by Ramalingaswami Fellowship from the Department of Biotechnology, Government of India and National Brain Research Centre core fund to S.B.

Authors declare no conflict of interest

Figure 1: Synaptic scaling is co-regulated by protein synthesis and degradation.

(A-C) mEPSC traces from hippocampal neurons treated with vehicle, lactacystin, anisomycin and both (A). Mean mEPSC amplitudes(B) and frequencies (C). n=13-15. *p<0.024, **p<0.01. (D-F) mEPSC traces from neurons treated with vehicle, bicuculline alone or in combination with lactacystin, anisomycin (D). Mean mEPSC amplitudes (E) and and frequencies (F). n=12–16. *p<0.01. ns, not significant. Data shown as Mean ± SEM. One Way ANOVA and Fisher's LSD. Scale as indicated.

Figure 2: Co-inhibition of protein synthesis and degradation restores hyperactivity driven reduction of synaptic AMPAR expression

(A-D) High magnification images of sGluA1 or sGluA2 (red), PSD95 (green) and sGluA1/PSD95 (A) or sGluA2/PSD95 (B) (merged) images from neurons treated with vehicle, bicuculline alone or in combination with lactacystin and anisomycin. Normalized intensity of sGluA1 (C) or sGluA2 (D) co-localized with PSD95 particles. n=56-57, sGluA1 and n=31-63, sGluA2. *p<0.01. (E-G) mEPSCs traces from hippocampal neurons treated with $GluA_{23y}$ either alone or in presence of bicuculline, lactacystin + anisomycin and bicuculline + lactacystin + anisomycin (E). Mean mEPSC amplitudes (F) and frequencies (G). n=10 - 13. ns, not significant. Data shown as Mean ± SEM. One Way ANOVA and Fisher's LSD. Scale as indicated. See also Figure S1.

Figure 3: RNA-dependent association between active proteasomes and translating polyribsomes

(A-D) Absorbance profile at 254nm (A_{254}) of fractionated cytoplasmic extracts from hippocampal tissue incubated without (A) or with RNAse (C) or with EDTA (E). Monosome (80S) or 60S Ribosome or Polysome fractions as indicated. Western blot analysis of fractions without (B) or with RNAse (D) or with EDTA (F) treatment showing distribution of translation regulators eIF4E and p70S6 Kinase; α7 subunit of 20S core and Rpt1, Rpt3, Rpt6 of 19S cap; miRISC proteins MOV10 and Trim32.

(G-H) A_{254} profile of fractionated cytoplasmic extract (G) and quantitation of catalytic activity of proteasomes present in alternate fractions from two polysome preparations (H). See also Figure S2.

Figure 4: Interaction between proteasome and actively translating RNA-associated polyribosomes.

(A) Proteasome associated protein complex was immunoprecipitated from hippocampal lysate using antibody against Rpt6 and Mouse IgG. Western blot of purified protein complex using antibodies against eEF2, p70S6 Kinase, phospho-p70S6 kinase.

(B-D) RiboTag mouse crossed with Camk2a promoter- driven Cre recombinase mouse results in deletion of wild-type Rpl22 ribosomal protein and replacement of HA tagged Rpl22 in forebrain excitatory neurons. A_{254} profile showing indicated fractions of Monosome and Polysome (C). Polysome fractions showing enrichement of HA-Rpl22 as detected by western blot using antibody against HA (D).

(E) HA-tagged Rpl22 containing polyribosome affinity purified using antibody against HA. Western blot analysis of affinity purified complex using antibodies against Rpt6, Trim32 and MOV10.

(F) MOV10 was immunoprecipitated from hippocampal lysate. Western blot analysis MOV10 immunoprecipitated protein complex showing co-precipitation of Trim32 with miRISC components MOV10 and Ago.

(G) Detection of HspA2 and Rpt6 in HA affinity purified protein complex from HA-Rpl22 expressing neurons by western blot using antibody against HspA2 and Rpt6 and HA.

Figure 5: Synthesis of Trim32 facilitates MOV10 degradation and requires activation of mTORC1

(A-C) Western blot analysis showing the expression of Trim32, MOV10 and Tuj1 from neurons treated with bicuculline with or without lactacystin, anisomycin or both (A). Quantitation of Trim32 (B) and MOV10 (C) expression. n=4. Data shown as Mean ± SEM. *$p<0.01$, **$p<0.03$, ***$p<0.02$ (B) and *$p<0.001$, **$p<0.006$, ***$p<0.02$ (C). ns, not significant. One Way ANOVA and Fisher's LSD.

(D-F) Western blot analysis of neurons infected with lentivirus expressing Trim32 or non-targetting control shRNA showing expression of Trim32, MOV10 and Tuj1 (D).

Quantitation of Trim32 (E) and MOV10 (F). n=5. Data shown as Mean ± SEM. *p<0.002 (E), *p<0.006 (F). Unpaired t-test with Welch's correction.

(G-I) Western blot analysis from neurons treated with bicuculline , Rapamycin or both. showing expression levels of Trim32, MOV10 and Tuj1 (G). Quantitation of Trim32 (H) MOV10 (I) expression. n=6. Data shown as Mean ± SEM. n=6. *p<0.0001, **p<0.0002, ***p<0.0009 (H) and *p<0.001 (I). ns, not significant. One Way ANOVA and Fisher's LSD. See also Figure S2.

(J-L) mEPSC traces from neurons treated with vehicle, bicuculline, rapamycin or both (J). Mean mEPSC amplitudes (K) and frequencies (L). n=8-9. *p<0.01. ns, not significant. Data shown as Mean ± SEM. One Way ANOVA and Fisher's LSD.

Figure 6: MOV10 regulates synaptic activity by modulating abundance of AMPAR expression at synapses.

(A-D) High magnification images of neurons transduced with lentivirus co-expressing EGFP and MOV10 or non-targetting shRNA showing expression of surface GluA1 (A) or GluA2 (C) (red),PSD95 (blue),GFP (green) and GFP/GluA1/PSD95 or GFP/GluA2/PSD95 (merged). Quantitation of normalized intensity of synaptic surface GluA1 (B) or GluA2 (D). n=26 - 30, GluA1; n=12 – 15, GluA2. Data shown as Mean ± SEM. *p<0.01. One Way ANOVA and Fisher's LSD. See also Figure S3.

(E-G) mEPSC traces from transduced neurons (E). Mean mEPSC amplitudes (F) and frequencies (G) n=12 – 13. *p<0.01. ns, not significant. Data shown as Mean ± SEM. One Way ANOVA.

Figure 7: Schematic representation showing maintenance of homeostatic synaptic activity by coordinated control of protein synthesis and degradation that modulates composition of miRISC.

References:

1. J. Burrone, V. N. Murthy, Synaptic gain control and homeostasis. *Curr. Opin. Neurobiol.* (2003) https:/doi.org/10.1016/j.conb.2003.09.007.
2. T. Keck, *et al.*, Integrating Hebbian and homeostatic plasticity: The current state of the field and future research directions. *Philos. Trans. R. Soc. B Biol. Sci.* (2017) https:/doi.org/10.1098/rstb.2016.0158.
3. G. G. Turrigiano, The dialectic of hebb and homeostasis. *Philos. Trans. R. Soc. B Biol. Sci.* (2017) https:/doi.org/10.1098/rstb.2016.0258.
4. G. G. Turrigiano, S. B. Nelson, Homeostatic plasticity in the developing nervous system. *Nat. Rev. Neurosci.* (2004) https:/doi.org/10.1038/nrn1327.
5. G. G. Turrigiano, K. R. Leslie, N. S. Desai, L. C. Rutherford, S. B. Nelson, Activity-dependent scaling of quantal amplitude in neocortical neurons. *Nature* (1998) https:/doi.org/10.1038/36103.
6. N. Vitureira, Y. Goda, The interplay between hebbian and homeostatic synaptic plasticity. *J. Cell Biol.* (2013) https:/doi.org/10.1083/jcb.201306030.
7. K. Pozo, Y. Goda, Unraveling mechanisms of homeostatic synaptic plasticity. *Neuron* (2010) https:/doi.org/10.1016/j.neuron.2010.04.028.
8. G. G. Turrigiano, The Self-Tuning Neuron: Synaptic Scaling of Excitatory Synapses. *Cell* (2008) https:/doi.org/10.1016/j.cell.2008.10.008.
9. G. W. Davis, HOMEOSTATIC CONTROL OF NEURAL ACTIVITY: From Phenomenology to Molecular Design. *Annu. Rev. Neurosci.* (2006) https:/doi.org/10.1146/annurev.neuro.28.061604.135751.
10. K. Ibata, Q. Sun, G. G. Turrigiano, Rapid Synaptic Scaling Induced by Changes in Postsynaptic Firing. *Neuron* (2008) https:/doi.org/10.1016/j.neuron.2008.02.031.
11. C. J. Wierenga, M. F. Walsh, G. G. Turrigiano, Temporal regulation of the expression locus of homeostatic plasticity. *J. Neurophysiol.* (2006) https:/doi.org/10.1152/jn.00107.2006.

12. C. J. Wierenga, K. Ibata, G. G. Turrigiano, Postsynaptic expression of homeostatic plasticity at neocortical synapses. *J. Neurosci.* (2005) https:/doi.org/10.1523/JNEUROSCI.5217-04.2005.

13. M. A. Sutton, A. M. Taylor, H. T. Ito, A. Pham, E. M. Schuman, Postsynaptic Decoding of Neural Activity: eEF2 as a Biochemical Sensor Coupling Miniature Synaptic Transmission to Local Protein Synthesis. *Neuron* (2007) https:/doi.org/10.1016/j.neuron.2007.07.030.

14. F. E. Henry, *et al.*, A unique homeostatic signaling pathway links synaptic inactivity to postsynaptic mTORC1. *J. Neurosci.* (2018) https:/doi.org/10.1523/JNEUROSCI.1843-17.2017.

15. F. E. Henry, *et al.*, Retrograde changes in presynaptic function driven by dendritic mTORC1. *J. Neurosci.* (2012) https:/doi.org/10.1523/JNEUROSCI.2149-12.2012.

16. M. A. Gainey, J. R. Hurvitz-Wolff, M. E. Lambo, G. G. Turrigiano, Synaptic scaling requires the GluR2 subunit of the AMPA receptor. *J. Neurosci.* (2009) https:/doi.org/10.1523/JNEUROSCI.3753-08.2009.

17. R. J. O'Brien, *et al.*, Activity-dependent modulation of synaptic AMPA receptor accumulation. *Neuron* (1998) https:/doi.org/10.1016/S0896-6273(00)80624-8.

18. V. Tatavarty, Q. Sun, G. G. Turrigiano, How to scale down postsynaptic strength. *J. Neurosci.* (2013) https:/doi.org/10.1523/JNEUROSCI.1676-13.2013.

19. T. C. Thiagarajan, M. Lindskog, R. W. Tsien, Adaptation to synaptic inactivity in hippocampal neurons. *Neuron* (2005) https:/doi.org/10.1016/j.neuron.2005.06.037.

20. M. A. Sutton, *et al.*, Miniature Neurotransmission Stabilizes Synaptic Function via Tonic Suppression of Local Dendritic Protein Synthesis. *Cell* (2006) https:/doi.org/10.1016/j.cell.2006.03.040.

21. D. V. Lissin, *et al.*, Activity differentially regulates the surface expression of synaptic AMPA and NMDA glutamate receptors. *Proc. Natl. Acad. Sci. U. S. A.* (1998) https:/doi.org/10.1073/pnas.95.12.7097.

22. Q. Hou, *et al.*, MicroRNA miR124 is required for the expression of homeostatic synaptic plasticity. *Nat. Commun.* (2015) https:/doi.org/10.1038/ncomms10045.

23. M. Letellier, *et al.*, MiR-92a regulates expression of synaptic GluA1-containing AMPA receptors during homeostatic scaling. *Nat. Neurosci.* (2014) https:/doi.org/10.1038/nn.3762.

24. M. Rajman, *et al.*, A microRNA-129-5p/Rbfox crosstalk coordinates homeostatic downscaling of excitatory synapses. *EMBO J.* (2017) https:/doi.org/10.15252/embj.201695748.

25. M. M. Silva, *et al.*, MicroRNA-186-5p controls GluA2 surface expression and synaptic scaling in hippocampal neurons. *Proc. Natl. Acad. Sci. U. S. A.* (2019) https:/doi.org/10.1073/pnas.1900338116.

26. S. Banerjee, P. Neveu, K. S. Kosik, A Coordinated Local Translational Control Point at the Synapse Involving Relief from Silencing and MOV10 Degradation. *Neuron* (2009) https:/doi.org/10.1016/j.neuron.2009.11.023.

27. P. J. Kenny, *et al.*, MOV10 and FMRP Regulate AGO2 Association with MicroRNA Recognition Elements. *Cell Rep.* (2014) https:/doi.org/10.1016/j.celrep.2014.10.054.

28. M. D. Ehlers, Activity level controls postsynaptic composition and signaling via the ubiquitin-proteasome system. *Nat. Neurosci.* (2003) https:/doi.org/10.1038/nn1013.

29. S. K. Jakawich, R. M. Neely, S. N. Djakovic, G. N. Patrick, M. A. Sutton, An essential postsynaptic role for the ubiquitin proteasome system in slow homeostatic synaptic plasticity in cultured hippocampal neurons. *Neuroscience* (2010) https:/doi.org/10.1016/j.neuroscience.2010.09.061.

30. C. T. Schanzenbächer, S. Sambandan, J. D. Langer, E. M. Schuman, Nascent Proteome Remodeling following Homeostatic Scaling at Hippocampal Synapses. *Neuron* (2016) https:/doi.org/10.1016/j.neuron.2016.09.058.

31. C. T. Schanzenbächer, J. D. Langer, E. M. Schuman, Time- and polarity-dependent proteomic changes associated with homeostatic scaling at central synapses. *Elife* (2018) https:/doi.org/10.7554/eLife.33322.

32. B. Bingol, E. M. Schuman, Activity-dependent dynamics and sequestration of proteasomes in dendritic spines. *Nature* (2006) https:/doi.org/10.1038/nature04769.

33. L. E. Ostroff, J. C. Fiala, B. Allwardt, K. M. Harris, Polyribosomes redistribute from dendritic shafts into spines with enlarged synapses during LTP in developing rat hippocampal slices. *Neuron* (2002) https:/doi.org/10.1016/S0896-6273(02)00785-7.

34. J. C. Schwamborn, E. Berezikov, J. A. Knoblich, The TRIM-NHL Protein TRIM32 Activates MicroRNAs and Prevents Self-Renewal in Mouse Neural Progenitors. *Cell* (2009) https:/doi.org/10.1016/j.cell.2008.12.024.

35. G. Meister, *et al.*, Identification of novel argonaute-associated proteins. *Curr. Biol.* (2005) https:/doi.org/10.1016/j.cub.2005.10.048.

36. X. M. Ma, J. Blenis, Molecular mechanisms of mTOR-mediated translational control. *Nat. Rev. Mol. Cell Biol.* (2009) https:/doi.org/10.1038/nrm2672.

37. E. Sanz, *et al.*, Cell-type-specific isolation of ribosome-associated mRNA from complex tissues. *Proc. Natl. Acad. Sci. U. S. A.* (2009) https:/doi.org/10.1073/pnas.0907143106.

38. T. Shigeoka, *et al.*, Dynamic Axonal Translation in Developing and Mature Visual Circuits. *Cell* (2016) https:/doi.org/10.1016/j.cell.2016.05.029.

39. A. M. Krichevsky, K. S. King, C. P. Donahue, K. Khrapko, K. S. Kosik, A microRNA array reveals extensive regulation of microRNAs during brain development. *RNA* (2003) https:/doi.org/10.1261/rna.5980303.

40. R. Fonseca, R. M. Vabulas, F. U. Hartl, T. Bonhoeffer, U. V. Nägerl, A Balance of Protein Synthesis and Proteasome-Dependent Degradation Determines the Maintenance of LTP. *Neuron* (2006) https:/doi.org/10.1016/j.neuron.2006.08.015.

41. M. E. Klein, P. E. Castillo, B. A. Jordan, Coordination between translation and degradation regulates inducibility of mGluR-LTD. *Cell Rep.* (2015) https:/doi.org/10.1016/j.celrep.2015.02.020.

42. C. Hanus, E. M. Schuman, Proteostasis in complex dendrites. *Nat. Rev. Neurosci.* (2013) https:/doi.org/10.1038/nrn3546.

43. C. P. Goold, R. A. Nicoll, Single-Cell Optogenetic Excitation Drives Homeostatic Synaptic Depression. *Neuron* (2010) https:/doi.org/10.1016/j.neuron.2010.09.020.

44. H. C. Tai, H. Besche, A. L. Goldberg, E. M. Schuman, Characterization of the brain 26S proteasome and its interacting proteins. *Front. Mol. Neurosci.* (2010) https:/doi.org/10.3389/fnmol.2010.00012.

45. R. Shalgi, *et al.*, Widespread Regulation of Translation by Elongation Pausing in Heat Shock. *Mol. Cell* (2013) https:/doi.org/10.1016/j.molcel.2012.11.028.

46. K. V. Ramachandran, *et al.*, Activity-Dependent Degradation of the Nascentome by the Neuronal Membrane Proteasome. *Mol. Cell* (2018) https:/doi.org/10.1016/j.molcel.2018.06.013.

47. G. H. Diering, R. L. Huganir, The AMPA Receptor Code of Synaptic Plasticity. *Neuron* (2018) https:/doi.org/10.1016/j.neuron.2018.10.018.

48. A. J. H. Yong, *et al.*, Tyrosine phosphorylation of the AMPA receptor subunit GluA2 gates homeostatic synaptic plasticity. *Proc. Natl. Acad. Sci.* (2020) https:/doi.org/10.1073/pnas.1918436117.

49. G. H. Diering, *et al.*, Homer1a drives homeostatic scaling-down of excitatory synapses during sleep. *Science (80-.).* (2017) https:/doi.org/10.1126/science.aai8355.

50. S. Kaech, G. Banker, Culturing hippocampal neurons. *Nat. Protoc.* (2006) https:/doi.org/10.1038/nprot.2006.356.

51 L. A. Schwarz, B. J. Hall, G. N. Patrick, Activity-dependent ubiquitination of GluA1 mediates a distinct AMPA receptor endocytosis and sorting pathway. *J. Neurosci.* (2010) https:/doi.org/10.1523/JNEUROSCI.3686-10.2010.

52. G. Stefani, C. E. Fraser, J. C. Darnell, R. B. Darnell, Fragile X mental retardation protein is associated with translating polyribosomes in neuronal cells. *J. Neurosci.* (2004) https:/doi.org/10.1523/JNEUROSCI.2306-04.2004.

Figure:1

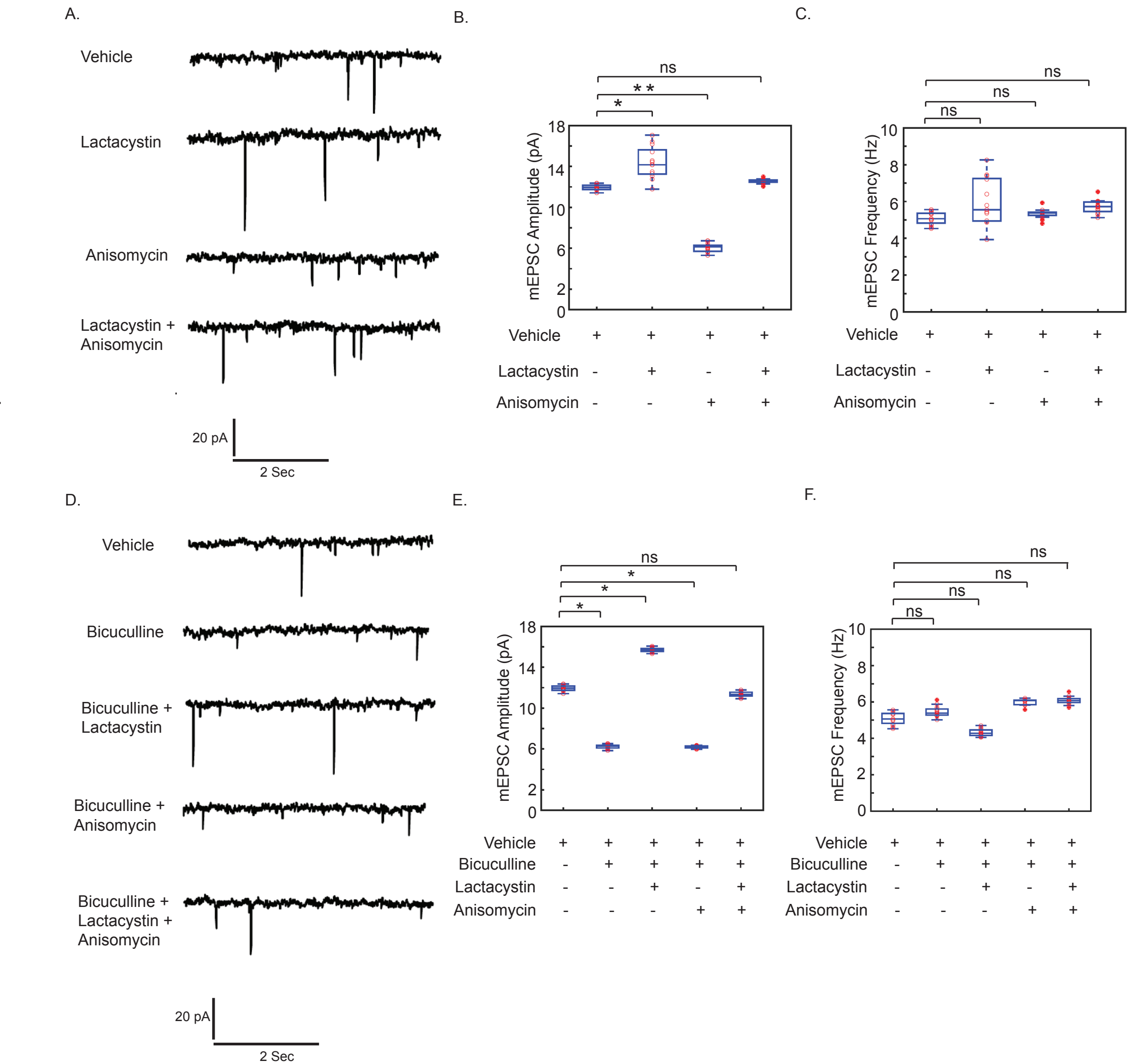
A.
Vehicle
Lactacystin
Anisomycin
Lactacystin + Anisomycin
20 pA
2 Sec
B.
ns
**
*
mEPSC Amplitude (pA)
18
14
10
6
2
0
Vehicle + + + +
Lactacystin - + - +
Anisomycin - - + +
C.
ns
ns
ns
mEPSC Frequency (Hz)
10
8
6
4
2
0
Vehicle + + + +
Lactacystin - + - +
Anisomycin - - + +
D.
Vehicle
Bicuculline
Bicuculline + Lactacystin
Bicuculline + Anisomycin
Bicuculline + Lactacystin + Anisomycin
20 pA
2 Sec
E.
ns
*
*
*
mEPSC Amplitude (pA)
18
14
10
6
2
0
Vehicle + + + + +
Bicuculline - + + + +
Lactacystin - - + - +
Anisomycin - - - + +
F.
ns
ns
ns
ns
mEPSC Frequency (Hz)
10
8
6
4
2
0
Vehicle + + + + +
Bicuculline - + + + +
Lactacystin - - + - +
Anisomycin - - - + +

Figure: 2

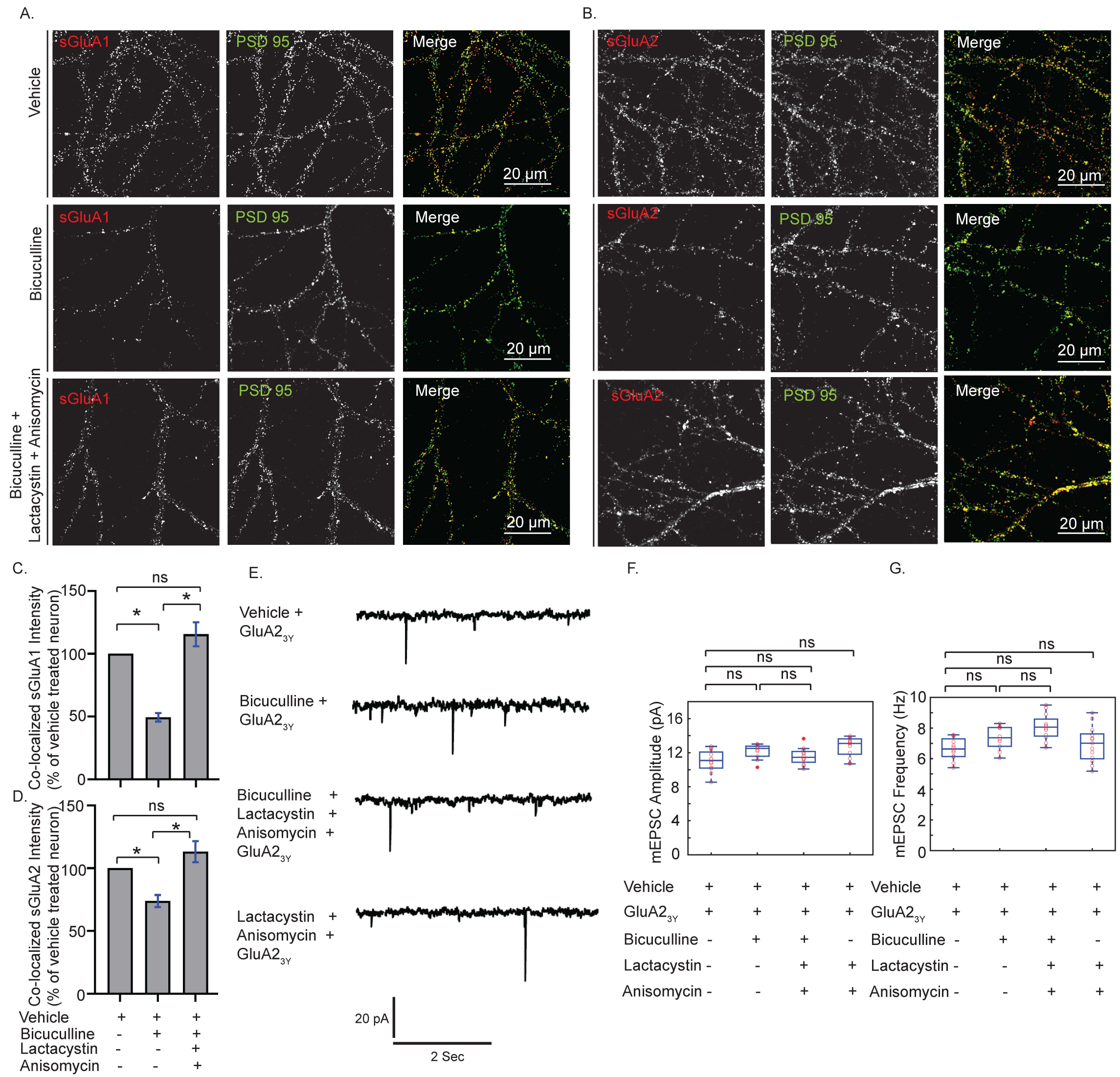
A.
B.
Vehicle
Bicuculline
Bicuculline + Lactacystin + Anisomycin
sGluA1
PSD 95
Merge
sGluA2
20 µm
C.
D.
Co-localized sGluA1 Intensity (% of vehicle treated neuron)
Co-localized sGluA2 Intensity (% of vehicle treated neuron)
ns
*
Vehicle + + +
Bicuculline - + +
Lactacystin - - +
Anisomycin - - +
E.
Vehicle + GluA2$_{3Y}$
Bicuculline + GluA2$_{3Y}$
Bicuculline + Lactacystin + Anisomycin + GluA2$_{3Y}$
Lactacystin + Anisomycin + GluA2$_{3Y}$
20 pA
2 Sec
F.
mEPSC Amplitude (pA)
G.
mEPSC Frequency (Hz)
Vehicle
GluA2$_{3Y}$
Bicuculline
Lactacystin
Anisomycin

Figure:3

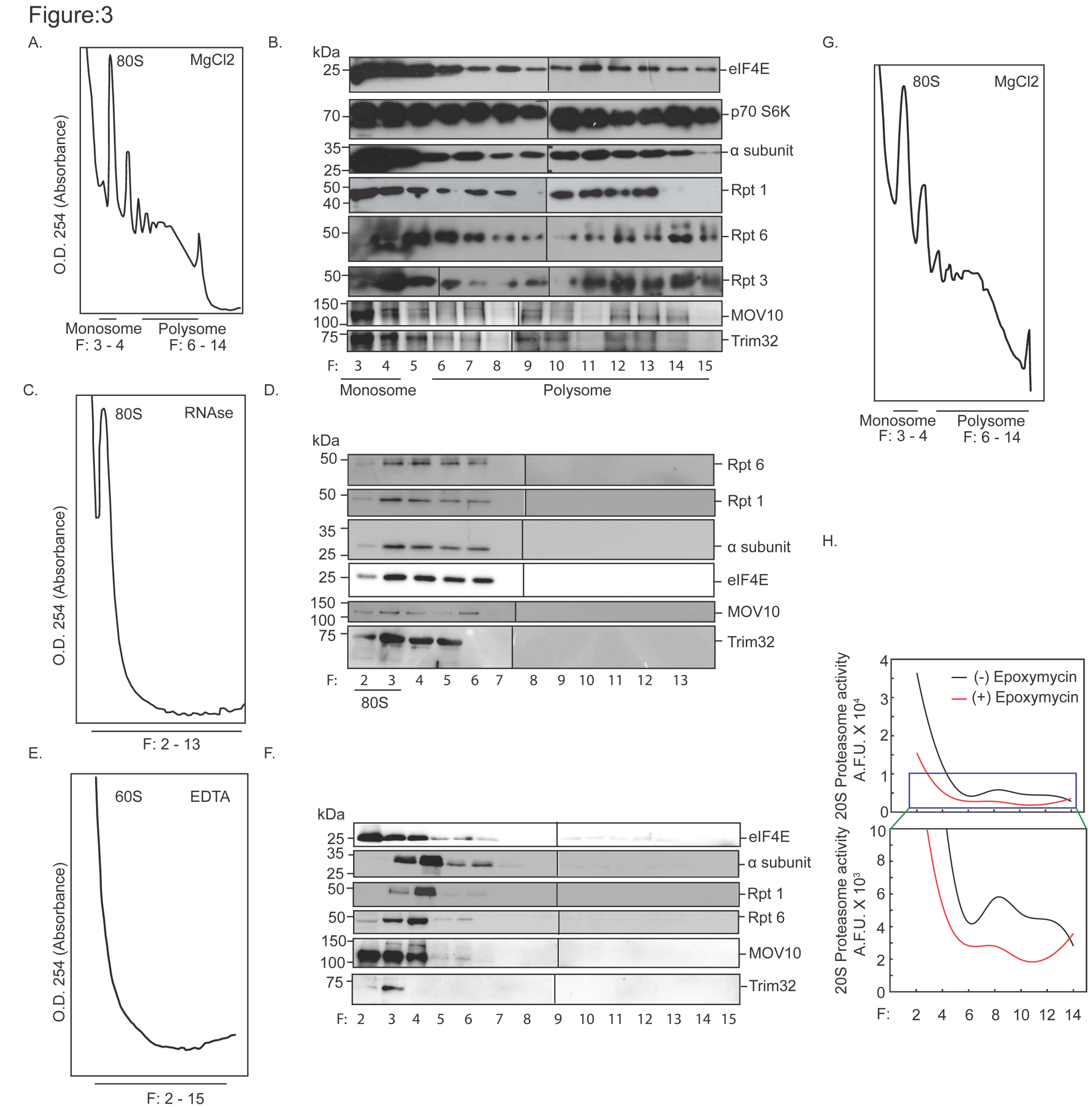
A.
80S
MgCl2
O.D. 254 (Absorbance)
Monosome
F: 3 - 4
Polysome
F: 6 - 14
B.
kDa
25
eIF4E
70
p70 S6K
35
25
α subunit
50
40
Rpt 1
50
Rpt 6
50
Rpt 3
150
100
MOV10
75
Trim32
F: 3 4 5 6 7 8 9 10 11 12 13 14 15
Monosome
Polysome
G.
80S
MgCl2
Monosome
F: 3 - 4
Polysome
F: 6 - 14
C.
80S
RNAse
O.D. 254 (Absorbance)
F: 2 - 13
D.
kDa
50
Rpt 6
50
Rpt 1
35
25
α subunit
25
eIF4E
150
100
MOV10
75
Trim32
F: 2 3 4 5 6 7 8 9 10 11 12 13
80S
H.
(-) Epoxymycin
(+) Epoxymycin
20S Proteasome activity
A.F.U. X 10⁴
20S Proteasome activity
A.F.U. X 10³
F: 2 4 6 8 10 12 14
E.
60S
EDTA
O.D. 254 (Absorbance)
F: 2 - 15
F.
kDa
25
eIF4E
35
25
α subunit
50
Rpt 1
50
Rpt 6
150
100
MOV10
75
Trim32
F: 2 3 4 5 6 7 8 9 10 11 12 13 14 15

Figure: 4

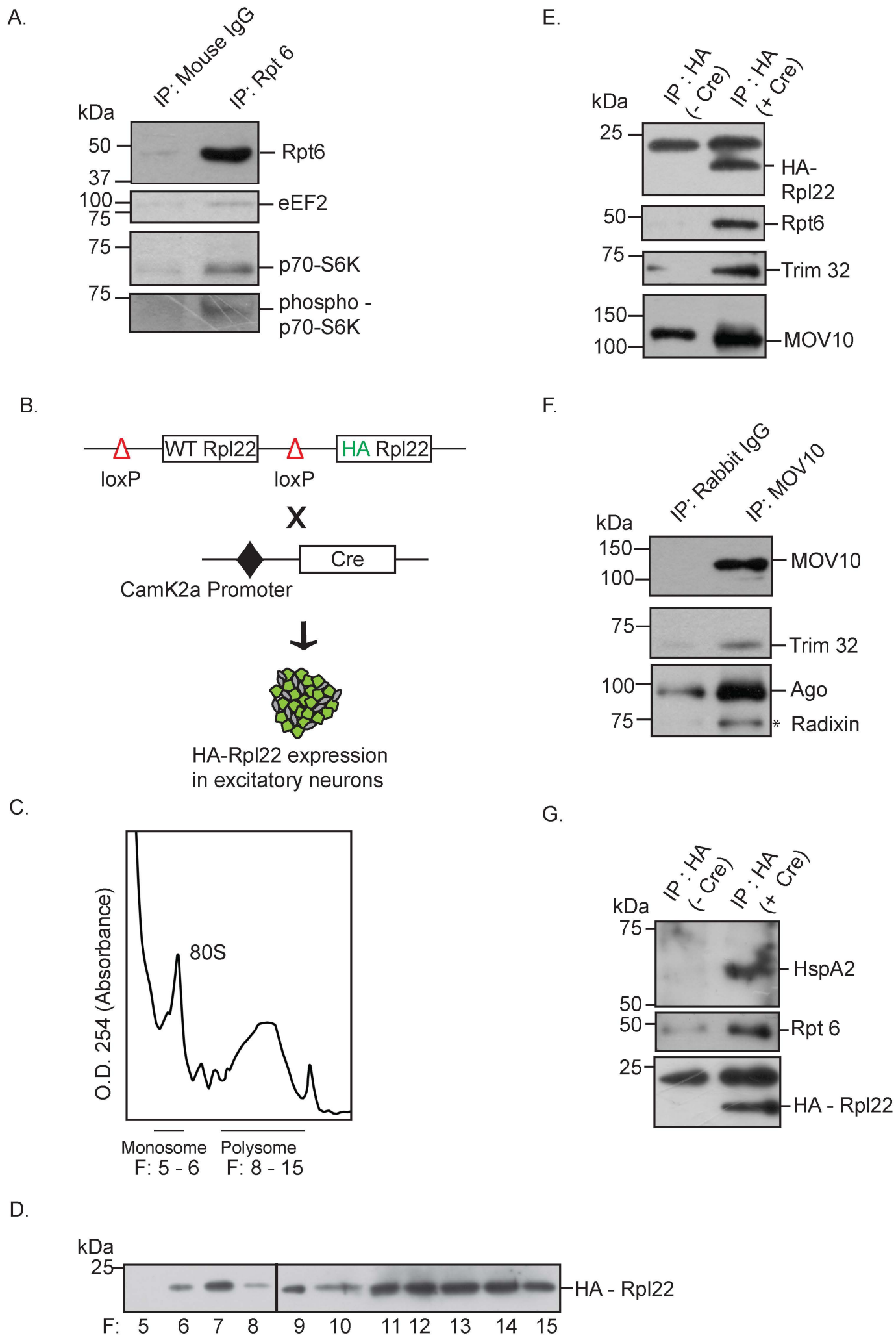
A.
IP: Mouse IgG
IP: Rpt 6
kDa
50
37
100
75
75
75
Rpt6
eEF2
p70-S6K
phospho - p70-S6K
B.
WT Rpl22
HA Rpl22
loxP
loxP
X
Cre
CamK2a Promoter
HA-Rpl22 expression in excitatory neurons
C.
O.D. 254 (Absorbance)
80S
Monosome F: 5 - 6
Polysome F: 8 - 15
D.
kDa
25
HA - Rpl22
F: 5 6 7 8 9 10 11 12 13 14 15
E.
IP : HA (- Cre)
IP : HA (+ Cre)
kDa
25
50
75
150
100
HA-Rpl22
Rpt6
Trim 32
MOV10
F.
IP: Rabbit IgG
IP: MOV10
kDa
150
100
75
100
75
MOV10
Trim 32
Ago
* Radixin
G.
IP : HA (- Cre)
IP : HA (+ Cre)
kDa
75
50
50
25
HspA2
Rpt 6
HA - Rpl22

Figure: 5

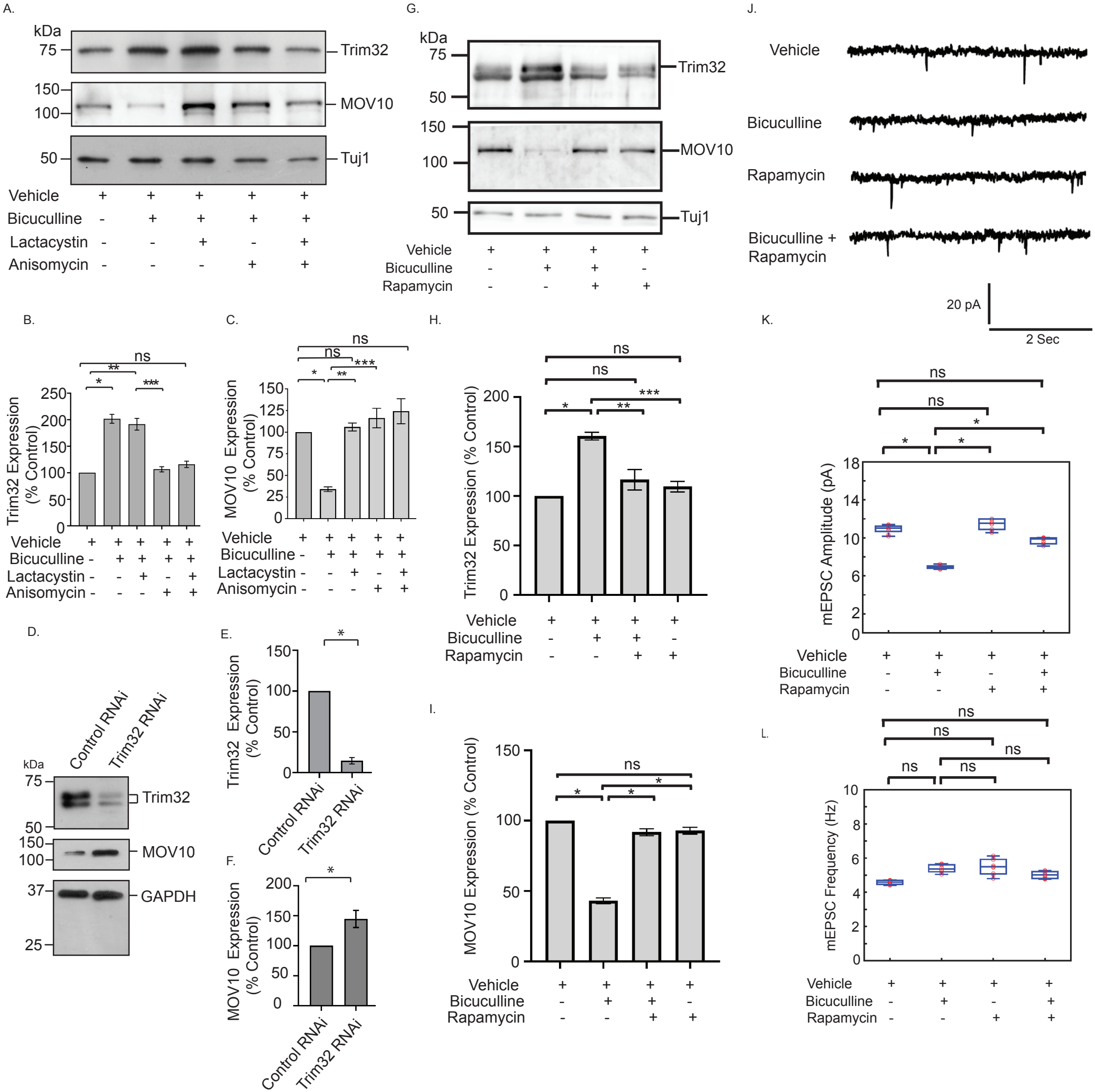
A.
kDa
75
150
100
50
Trim32
MOV10
Tuj1
Vehicle + + + + +
Bicuculline - + + + +
Lactacystin - - + - +
Anisomycin - - - + +
G.
kDa
75
50
150
100
50
Trim32
MOV10
Tuj1
Vehicle + + + +
Bicuculline - + + -
Rapamycin - - + +
J.
Vehicle
Bicuculline
Rapamycin
Bicuculline + Rapamycin
20 pA
2 Sec
B.
Trim32 Expression (% Control)
ns
**
*
***
Vehicle + + + + +
Bicuculline - + + + +
Lactacystin - - + - +
Anisomycin - - - + +
C.
MOV10 Expression (% Control)
ns
ns
***
*
**
Vehicle + + + + +
Bicuculline - + + + +
Lactacystin - - + - +
Anisomycin - - - + +
H.
Trim32 Expression (% Control)
ns
ns
***
*
**
Vehicle + + + +
Bicuculline - + + -
Rapamycin - - + +
K.
mEPSC Amplitude (pA)
ns
ns
*
*
*
Vehicle + + + +
Bicuculline - + - +
Rapamycin - - + +
D.
Control RNAi
Trim32 RNAi
kDa
75
50
150
100
37
25
Trim32
MOV10
GAPDH
E.
Trim32 Expression (% Control)
*
Control RNAi
Trim32 RNAi
F.
MOV10 Expression (% Control)
*
Control RNAi
Trim32 RNAi
I.
MOV10 Expression (% Control)
ns
*
*
Vehicle + + + +
Bicuculline - + + -
Rapamycin - - + +
L.
mEPSC Frequency (Hz)
ns
ns
ns
ns
ns
Vehicle + + + +
Bicuculline - + - +
Rapamycin - - + +

Figure: 6

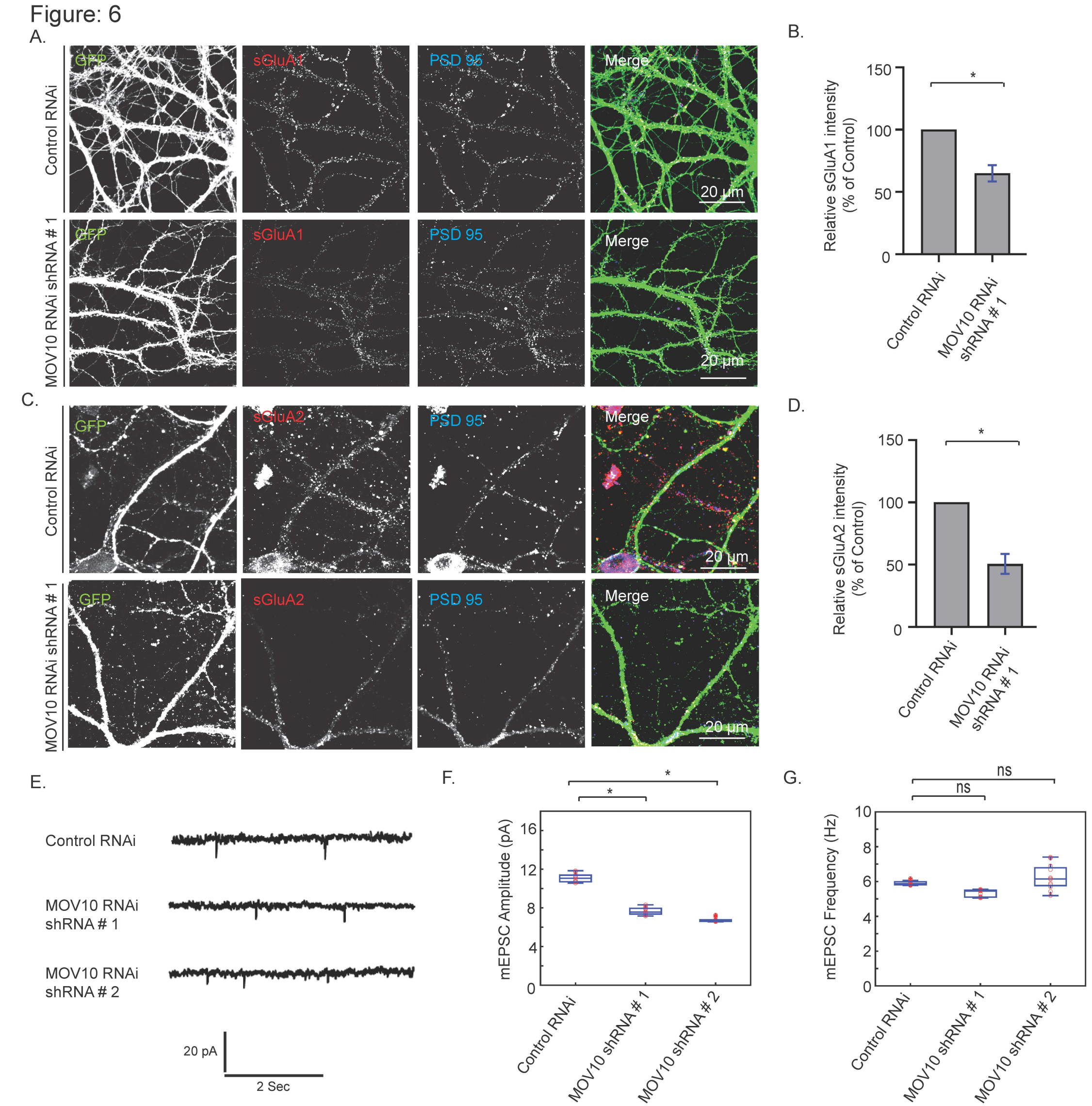
A.
Control RNAi
MOV10 RNAi shRNA # 1
GFP
sGluA1
PSD 95
Merge
20 µm
B.
Relative sGluA1 intensity (% of Control)
150
100
50
0
*
Control RNAi
MOV10 RNAi shRNA # 1
C.
sGluA2
D.
Relative sGluA2 intensity (% of Control)
E.
Control RNAi
MOV10 RNAi shRNA # 1
MOV10 RNAi shRNA # 2
20 pA
2 Sec
F.
mEPSC Amplitude (pA)
16
12
8
4
0
MOV10 shRNA # 1
MOV10 shRNA # 2
G.
mEPSC Frequency (Hz)
10
8
6
4
2
0
ns

Figure: 7

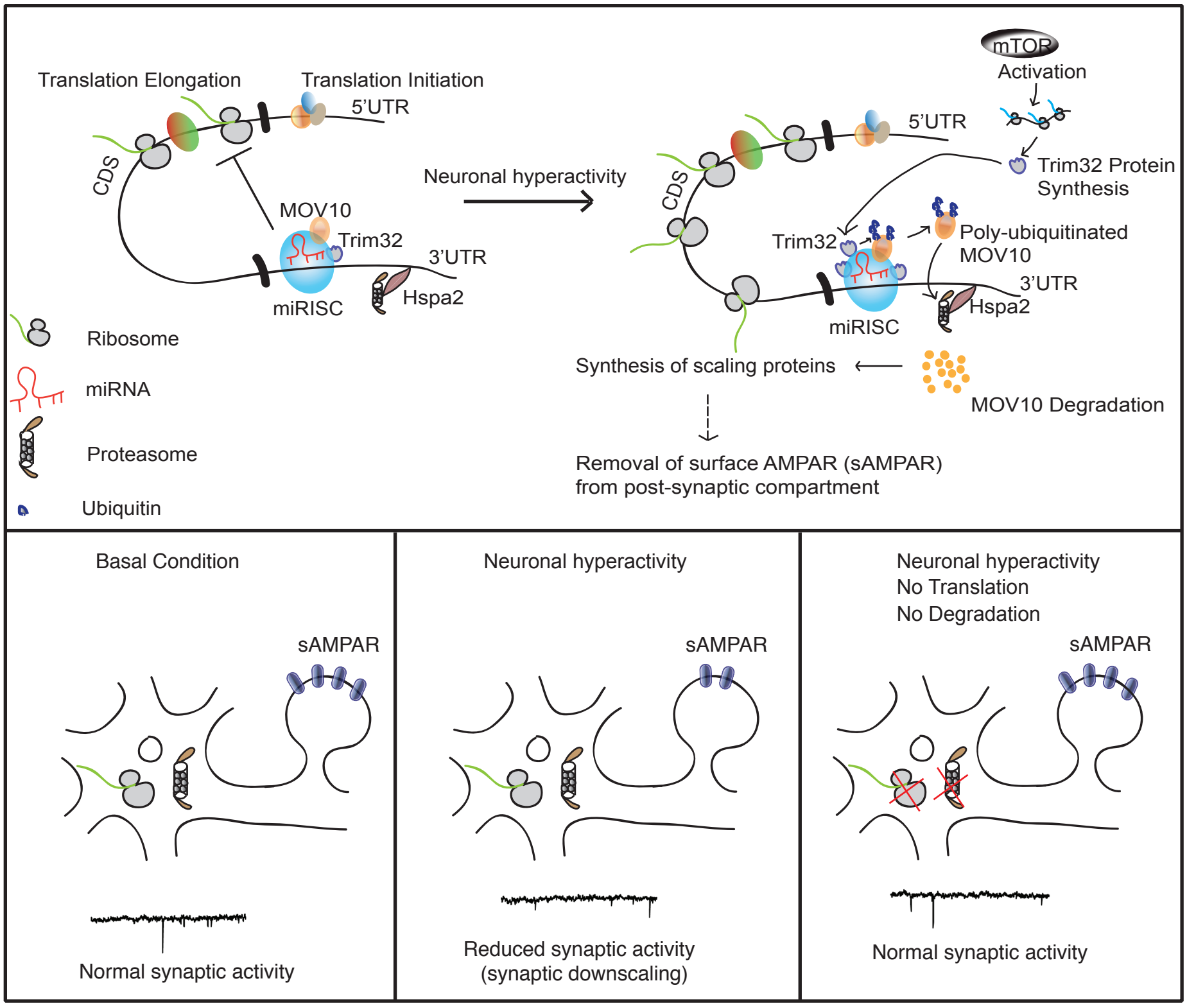
Translation Elongation
Translation Initiation
5'UTR
CDS
MOV10
Trim32
3'UTR
miRISC
Hspa2
Neuronal hyperactivity
mTOR
Activation
Trim32 Protein Synthesis
Poly-ubiquitinated MOV10
Synthesis of scaling proteins
MOV10 Degradation
Removal of surface AMPAR (sAMPAR) from post-synaptic compartment
Ribosome
miRNA
Proteasome
Ubiquitin
Basal Condition
sAMPAR
Normal synaptic activity
Neuronal hyperactivity
Reduced synaptic activity (synaptic downscaling)
Neuronal hyperactivity
No Translation
No Degradation
Normal synaptic activity